OUTFLOW VERSUS INFALL IN SPIRAL GALAXIES: METAL ABSORPTION IN THE HALO OF NGC 891

The Astrophysical Journal, 766:57 (6pp), 2013 March 20 doi:10.1088/0004-637X/766/1/57

OUTFLOW VERSUS INFALL IN SPIRAL GALAXIES: METAL ABSORPTION IN THE HALO OF NGC 891

Joel N. Bregman[1], Eric D. Miller[2], Patrick Seitzer[1], C. R. Cowley[1], and Matthew J. Miller[1]
[1] Department of Astronomy, University of Michigan, Ann Arbor, MI 48105, USA; jbregman@umich.edu
[2] Kavli Institute for Astrophysics and Space Research, Massachusetts Institute of Technology, Cambridge, MA 02139, USA
Received 2010 July 8; accepted 2013 January 7; published 2013 March 7

ABSTRACT

Gas accreting onto a galaxy will be of low metallicity while halo gas due to a galactic fountain will be of near-solar metallicity. We test these predictions by measuring the metal absorption line properties of halo gas 5 kpc above the plane of the edge-on galaxy NGC 891, using observations taken with *HST*/STIS toward a bright background quasar. Metal absorption lines of Fe II, Mg II, and Mg I in the halo of NGC 891 are clearly seen, and when combined with recent deep H I observations, we are able to place constraints on the metallicity of the halo gas for the first time. The H I line width defines the line broadening, from which we model opacity effects in these metal lines, assuming that the absorbing gas is continuously distributed in the halo. The gas-phase metallicities are $[Fe/H] = -1.18 \pm 0.07$ and $[Mg/H] = -0.23 + 0.36/ - 0.27$ (statistical errors) and this difference is probably due to differential depletion onto grains. When corrected for such depletion using Galactic gas as a guide, both elements have approximately solar or even supersolar abundances. This suggests that the gas is from the galaxy disk, probably expelled into the halo by a galactic fountain, rather than from accretion of intergalactic gas, which would have a low metallicity. The abundances would be raised by significant amounts if the absorbing gas lies in a few clouds with thermal widths smaller than the rotational velocity of the halo. If this is the case, both the abundances and [Mg/Fe] would be supersolar.

Key words: galaxies: individual (NGC 891) – galaxies: ISM – galaxies: kinematics and dynamics

Online-only material: color figures

1. INTRODUCTION

The formation of galactic disks occurs because gas with net angular momentum is accreted into a potential well before forming stars (e.g., review by Silk & Mamon 2012). The accretion can occur in two forms, where the gas is either at the temperature of the potential well (hot), or well below that temperature. If the gas is hot, radiative cooling leads to the creation of cool gas near the bottom of the potential well (the cooling flow model). Alternatively, the gas might already be cool (e.g., H I) falling nearly ballistically onto the disk (cold flows), where it probably shocks and radiatively cools before settling down onto the disk.

One or perhaps both of these processes were active when the galaxy disk formed and most of the disk stars were produced, typically 5–12 Gyr ago. In addition, accretion may be going on today in local galaxies at modest accretion rates. Gathering observational evidence for accretion today is of considerable importance since understanding accretion today can provide insights into the physics surrounding disk formation and evolution.

Both hot and cold gas is seen in the vicinity or extremities of galaxies and it could be accretion material. Examples of this are the high-velocity clouds of neutral hydrogen around the Milky Way (Wakker & van Woerden 1997) or M31 (Westmeier et al. 2005) and the hot X-ray-emitting atmospheres around edge-on spiral galaxies (Bregman & Pildis 1994; Strickland et al. 2004; Tüllmann et al. 2006; Li & Wang 2013). The X-ray-emitting halos of galaxies are largely related to the degree and extent of star formation in the disk, so this component is most likely due to a galactic fountain (Tüllmann et al. 2006). The situation with neutral gas likely points to at least two components: a galactic fountain origin for the intermediate-velocity clouds (and some high-velocity clouds) of H I and the accretion of extragalactic H I clouds, either from nearby dwarf companions (e.g., the Magellanic Stream from the Large Magellanic Cloud and Small Magellanic Cloud) or through condensation out of an extensive, dilute hot halo (much larger than 10 kpc and as yet unobserved in X-rays; Peek et al. 2008; Miller et al. 2009, and references therein).

Metallicity can provide insights into these processes since galactic gas will be enriched; gas torn from dwarf galaxies is of lower metallicity, while condensations from a large dilute halo may be close to primordial. Provided that these components can be separated either spatially or in velocity space, metallicities can identify their relative importance. The value of this approach is indicated by absorption line Milky Way studies, where some halo high-velocity clouds are found to have low metallicity (0.3 solar), demonstrating that some extragalactic gas is being accreted by the Milky Way (Wakker 2004). Until now, similar observations have not been possible for external galaxies, as it would require a background source such as an active galactic nucleus (AGN) to be projected behind the halo of an edge-on galaxy. Exactly that situation exists for an AGN that lies far behind the edge-on galaxy, NGC 891, where the AGN is projected 5 kpc from the galactic plane in the inner part of the galaxy (see Figure 1).

The edge-on galaxy NGC 891 is similar to the Milky Way in galaxy type and optical luminosity and it lies close enough (10 Mpc) that it has been mapped extensively in several interstellar medium (ISM) components, including H I, X-ray-emitting gas, and warm ionized gas (Rand et al. 1990; Bregman & Pildis 1994; Rand 1997; Swaters et al. 1997; Heald et al. 2006). A heroic 21 cm observation (Oosterloo et al. 2007) is deep enough to map low column densities to heights as great as 22 kpc above the plane, and $10^9\,M_\odot$ of H I gas lies in the halo. They argue that the H I halo is a combination of infalling material and a galactic fountain. Their H I map covers the region

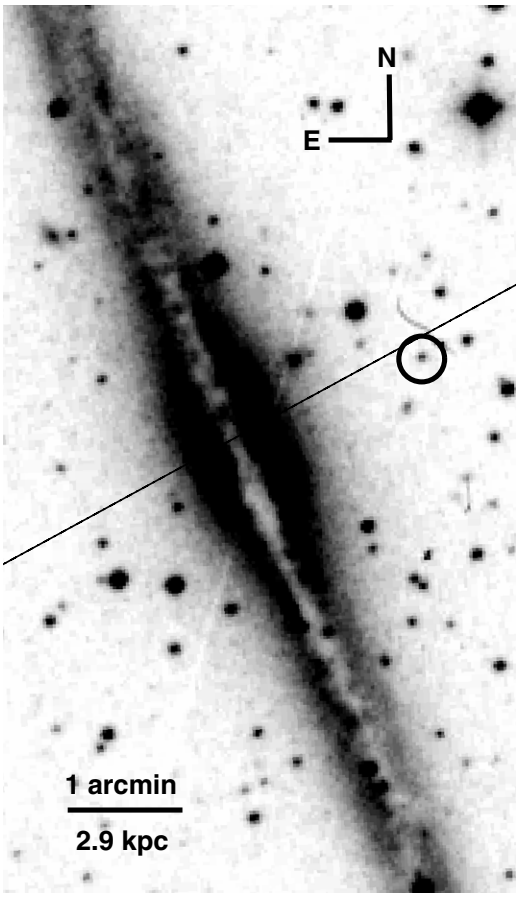

Figure 1. Edge-on galaxy NGC 891 with the background AGN marked with a circle. The AGN lies 106″ (5.1 kpc) from the midplane and 8″ (340 pc) from the minor axis, which is estimated from the H I data of Oosterloo et al. (2007) and marked here by a line.

of the AGN, so the H I column density along that sight line is known. Their H I study leads to an essential improvement in our original analysis (Miller et al. 2000), since, by measuring the column density of metal lines, we can now determine the metallicity of the halo gas. In the following sections, we present the *Hubble Space Telescope* (*HST*) spectroscopic observations, the resulting column density, and the metallicity implied. We conclude with a summary and interpretation of these results.

2. OBSERVATIONS AND DATA ANALYSIS

The background AGN that we observed with *HST*/STIS was identified as an X-ray source in a *ROSAT* image at J2000 coordinates R.A., decl. = $02^{h}22^{m}24\overset{s}{.}45$, $+42^{\circ}21'38\overset{''}{.}8$. The discovery technique, described in Knezek & Bregman (1998), used follow-up optical spectroscopy with the MDM 2.4 m telescope. A series of five 600 s exposures was obtained using the Modular Spectrograph on the MDM 2.4 m Hiltner telescope during fall 1996. The 85 mm camera with a 600 l mm^{-1} grating was used in first order with a thinned, backside illuminated SITe CCD. The sampling was 4.7 Å pixel^{-1}. Only the wavelength range of 3800–7600 Å is considered to prevent effects from overlapping spectral orders. The spectrophotometric standard star Feige 34 was used to flux calibrate the combined spectrum. However, the night was not photometric and thus only relative fluxes are available.

These spectroscopic observations revealed this X-ray source near NGC 891 to be an AGN that is projected upon the galaxy's

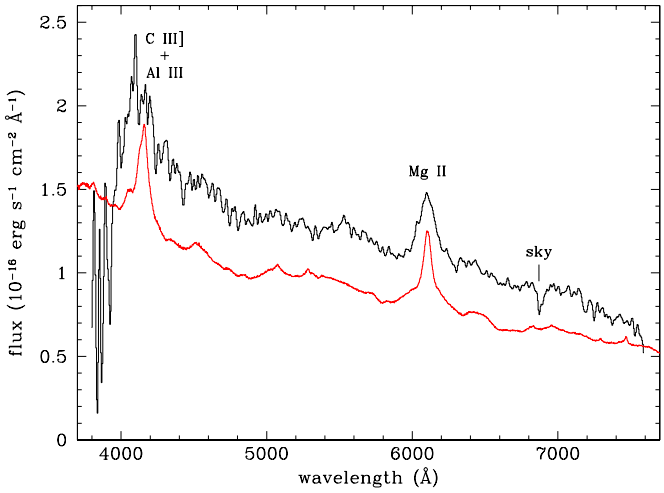

Figure 2. Optical spectrum (black) of the quasar taken with the MDM 2.4 m telescope. The SDSS composite quasar spectrum (red; Vanden Berk et al. 2001) is shown for comparison, redshifted to $z = 1.18$.

(A color version of this figure is available in the online journal.)

halo only 106″ (5.0 kpc) from the disk and in the inner part of the galaxy, 11″ along the disk direction ($r = 0.5$ kpc); it has $V = 18.7$ and $z = 1.18$ (Miller et al. 2000). The optical discovery spectrum is shown in Figure 2, which clearly identifies this as a broad-line quasar. This source was also identified by the Serendipitous Extragalactic X-Ray Source Identification program as CXOSEXSI J022224.3+422139 (Harrison et al. 2003), and follow-up optical spectroscopy in that program confirms our redshift determination and classification (Eckart et al. 2006). We note that no other nearby edge-on galaxies in our discovery program had bright AGNs within their halos, making this a singular target.

The metal line absorption data for this project were obtained with the Space Telescope Imaging Spectrograph (STIS) on board *HST* on 2000 September 6; the QSO was observed for a total of 13.2 ks over the span of 10 orbits. These observations used the $52'' \times 0\overset{''}{.}5$ aperture, NUV-MAMA detector, and G230L grating centered on 2376 Å. With this setup, the data cover a usable spectral range from 1750 to 3150 Å with a dispersion of 1.58 Å pixel^{-1}. The spectral resolution is 3.3 Å (413 km s^{-1}) FWHM at 2400 Å.

The individual exposures were scaled by the exposure time and combined. We identified the continuum (including QSO emission lines) along the lines described in the *HST* Quasar Absorption Line Key Project (Schneider et al. 1993). Figure 3 shows the combined spectrum along with the continuum fit and propagated 3σ errors. The resulting spectrum was searched for absorption features using the automated absorption line search algorithm available in the Key Project software. The procedure followed was identical to that described in Miller et al. (2002). Detected absorption lines were verified by eye. We also used SPECFIT (within STSDAS) and the fitting procedures within Origin Pro 8.5 to extract equivalent widths, obtaining similar results. It is essential to use the true instrumental line shape rather than just a Gaussian, otherwise one will obtain systematically smaller equivalent widths.

The QSO spectrum lacks the bright emission lines usually associated with such objects, and in fact shows complex absorption in the Lyβ and O VI emission line region (near 2240 Å). Corresponding absorption is seen near the very weak Lyα emission line (2650 Å) and the region where we expect N V emission

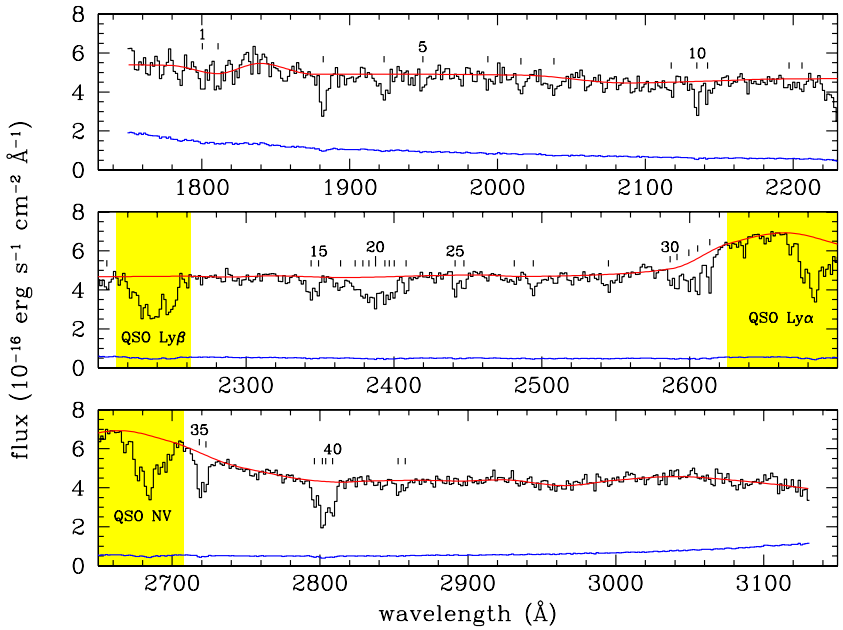

Figure 3. *HST* STIS/NUV spectrum of the QSO behind NGC 891. The red line shows the QSO continuum fit, the blue line shows the 3σ uncertainty. Tick marks indicate detected absorption features which correspond to entries in Table 1. The three broad absorption regions marked in yellow near 2240, 2600, and 2680 Å are due to QSO absorption, and have been ignored in the line searching and analysis.

(A color version of this figure is available in the online journal.)

(2700 Å). Indeed, the C III] + Al III peak in the optical spectrum (see Figure 2) also appears weaker than the composite quasar spectrum. The Mg II line, while fairly strong, lacks the narrow component seen in the composite. It is well fit by a Gaussian with FWHM $= 136.3 \pm 4.7$ Å (6680 ± 230 km s^{-1}). A detailed QSO classification requires additional spectroscopic analysis from a broader UV and optical band, and since we are only interested in the quasar as a background light source, such analysis is beyond the scope of the current work. Due to the complexities of the QSO Lyα and Lyβ features, we have excluded these regions from our analysis.

A number of absorption features were found with greater than 3σ significance; these are marked in Figure 3 and listed in Table 1 along with the best-fit line centers and equivalent widths. Due to the poor spectral resolution, each detected line was unresolved and we are unable to constrain the intrinsic line widths. To identify the absorbers, we first noted the expected Galactic and NGC 891 lines. We clearly see the strong Mg II λλ2796, 2803 doublet from NGC 891, although it is partially blended with its Galactic counterpart. The Fe II λ2344 line is detected in both the Galaxy and NGC 891 without contamination. Unfortunately, there is severe blending of the Fe II λλ2374, 2383, likely with Lyα forest lines. The best-fit decomposition is given in Table 1 (17–24) but we cannot obtain unique equivalent widths for these two lines at above 3σ, so they are not used in the determination of the Fe II column density. Similarly, line blending in 2570–2610 Å while less severe, caused unacceptably large systematic uncertainties for the Fe II λλ2587, 2600 lines, so the only line used for the analysis of the Fe II column is the λ2344 line. We note that had we used these other lines, a larger Fe II column density and metallicity would have resulted.

The remaining lines did not match any expected metal resonance absorption lines from the Galaxy or NGC 891, and they were taken to be intervening absorption systems. A simple matching procedure was implemented to identify single systems with multiple features. We discover a strong absorber at $z = 0.756$ with lines from Lyα, Lyβ, O VI λ1032, Si III λ1206, Si IV λλ1393, 1402, and C IV λλ1548, 1550. The measured equivalent widths of these species are similar to those for other C IV absorption systems identified in the literature (e.g., Sargent et al. 1988). The remaining absorption lines were taken to be Lyβ if a corresponding Lyα feature at the same redshift could be identified, otherwise they were assumed to be Lyα from intervening clouds. These results are included in Table 1 for completeness, but they will not be discussed further in the present work.

The wavelengths of the detected Galactic lines were not consistent with zero velocity, indicating a wavelength zero-point offset likely due to the source not being centered in the STIS aperture. We estimated an offset of -1.6 ± 0.6 Å from the best-fit centers of the clean Galactic absorption lines, assuming that they were at $v_r = 0$ km s^{-1}. This corresponds to about 1 pixel or 0.″025, larger than the nominal pointing error of 0.″01 (with no source acquisition peak-up), but not uncommon. We adjusted the spectrum and measured line centers to correct for this offset; those changes are reflected in Table 1 and Figure 3. The lines from NGC 891 are largely consistent with the measured systemic velocity of +528 km s^{-1}, which is also close to the measured H I velocity at this location above the disk (Oosterloo et al. 2007).

Clean detections of Fe II λ2344 and Mg II λ2803 from the halo of NGC 891 allow us to estimate column densities for these species. The Mg I λ2853 absorption line is detected at 5σ at the Milky Way velocity but only at 3σ from NGC 891, so we treat it as an upper limit. To obtain column densities requires corrections for the optical depth of the lines. There are not enough lines to fit a curve of growth for any one ion, from which a Doppler broadening parameter would be obtained. Fortunately, these ions and H I should be cospatial and the Doppler broadening parameter is available directly from the 21 cm H I observations, which are optically thin and have

Table 1
Discrete AVCs: General Properties

ID[a]	$\lambda_{obs} \pm \sigma$ (Å)	$W_\lambda \pm \sigma$ (Å)	Species	z or v[b]	System
1	1800.38 ± 0.75	0.98 ± 0.40	Lyβ	0.756	C IV absorber
2	1810.99 ± 0.78	0.88 ± 0.41	O VI λ1032	0.756	C IV absorber
3	1882.23 ± 0.32	2.56 ± 0.30	Lyα	0.548	···
4	1923.26 ± 0.63	1.62 ± 0.29	Lyα	0.582	···
5	1949.49 ± 0.82	0.85 ± 0.28	Lyα	0.604	···
6	1993.44 ± 0.70	0.68 ± 0.25	Lyβ	0.945	···
7	2015.92 ± 0.59	1.11 ± 0.24	Lyβ	0.969	···
8	2038.19 ± 0.56	1.05 ± 0.23	Lyα	0.677	···
9	2117.58 ± 0.64	0.75 ± 0.21	Si III λ1207	0.756	C IV absorber
10	2134.82 ± 0.22	1.94 ± 0.18	Lyα	0.756	C IV absorber
11	2142.02 ± 0.35	1.13 ± 0.19	Lyβ	1.094	···
12	2197.10 ± 0.33	0.62 ± 0.18	Lyα	0.807	···
13	2205.94 ± 0.58	0.77 ± 0.18	Lyβ	1.150	···
14	2344.08 ± 0.26	1.35 ± 0.14	Fe II λ2344	−17 ± 33	MW
15	2348.98 ± 0.83	0.83 ± 0.14	Fe II λ2344	+609 ± 106	NGC 891
16	2363.89 ± 0.74	0.80 ± 0.16	Lyα	0.945	···
17	2373.85 ± 0.53	0.81 ± 0.16[B]	Fe II λ2374	−76 ± 66	MW
18	2379.10 ± 0.38	1.08 ± 0.17[B]	Fe II λ2374	+585 ± 47	NGC 891
19	2383.14 ± 0.18	1.11 ± 0.17[B]	Fe II λ2383	+47 ± 22	MW
20	2387.52 ± 0.40	1.64 ± 0.15[B]	Fe II λ2383	+598 ± 50	NGC 891
21	2393.94 ± 0.15	1.38 ± 0.16	Lyα	0.969[b]	···
22	2396.87 ± 1.05	0.60 ± 0.20	Lyα	0.972[b]	···
23	2400.33 ± 0.34	1.07 ± 0.24	Lyα	0.974[b]	···
24	2408.24 ± 0.30	0.97 ± 0.15	Lyα	0.981	···
25	2441.44 ± 0.32	1.03 ± 0.15	Lyα	1.008	···
26	2447.25 ± 0.39	0.78 ± 0.15	Si IV λ1394	0.756	C IV absorber
27	2481.41 ± 0.88	0.59 ± 0.16	Lyα	1.041	···
28	2494.33 ± 0.11	1.12 ± 0.14	Lyα	1.052	···
29	2545.15 ± 0.41	1.03 ± 0.14	Lyα	1.094	···
30	2586.68 ± 0.42	0.67 ± 0.14[B]	Fe II λ2587	+3 ± 49	MW
31	2591.48 ± 0.29	1.19 ± 0.14[B]	Fe II λ2587	+560 ± 33	NGC 891
32	2599.39 ± 0.25	1.41 ± 0.13[B]	Fe II λ2600	−90 ± 28	MW
33	2605.38 ± 0.32	1.87 ± 0.12[B]	Fe II λ2600	+600 ± 36	NGC 891
34	2613.48 ± 0.17	1.75 ± 0.12	Lyα	1.150	···
35	2718.44 ± 0.15	2.01 ± 0.13	C IV λ1548	0.756	C IV absorber
36	2722.93 ± 0.21	1.56 ± 0.13	C IV λ1551	0.756	C IV absorber
37	2796.12 ± 0.24	1.56 ± 0.16	Mg II λ2796	−24 ± 25	MW
38	2801.57 ± 0.28	2.31 ± 0.61	Mg II λ2796	+559 ± 30	NGC 891
39	2803.79 ± 0.80	1.26 ± 0.58	Mg II λ2804	+27 ± 86	MW
40	2808.57 ± 0.20	2.28 ± 0.16	Mg II λ2804	+538 ± 21	NGC 891
41	2852.81 ± 0.47	0.83 ± 0.17	Mg I λ2853	−15 ± 49	MW
42	2857.59 ± 0.76	0.50 ± 0.17	Mg I λ2853	+485 ± 79	NGC 891

Notes.
[a] ID values correspond to the lines marked in Figure 3.
[b] Values with ± 1σ errors indicate velocities in km s^{-1}; other values are redshifts.
[B] Indicates blending that makes the EW values not sufficiently reliable for analysis.

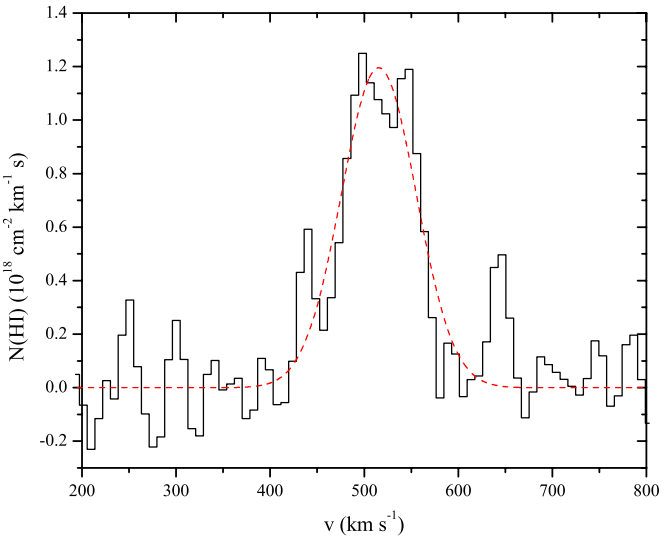

Figure 4. H I 21 cm emission spectrum through the halo of NGC 891, in the direction of the QSO. The vertical axis shows H I column density per km s^{-1}. The red dashed line traces the best-fit Gaussian profile, with a width of 93 ± 8 km s^{-1} FWHM. Data are from Oosterloo et al. (2007).
(A color version of this figure is available in the online journal.)

excellent velocity resolution. From the data that were obtained by Oosterloo et al. (2007), an H I spectrum was extracted at the location of the background AGN (see Figure 4). The spectrum shows a distribution that is typical of a rotating disk, having a flat-top profile with modest double-horns. To simplify matters, we fit the profile with a Gaussian where the FWHM = 93 ± 8 km s^{-1}. From the zero-moment map, the total H I column along this line of sight is 1.3×10^{20} cm^{-2}. With this column and line width, the optical depth at line center may be quite significant, depending upon the elemental abundances, since depletion on to grains may be important.

To infer the column densities for Fe II λ2344 and Mg II λ2803, we need to correct for optical depth effects, along with the ionization fraction. When the optical depth is small, the conversion is linear and independent of the number of components. However, for significant optical depths, the result depends not only on the equivalent width, the f value, and the Doppler parameter, it depends on whether there are multiple components. The existence of multiple components as well as their properties cannot be resolved with our data, so we proceed by assuming that the gas is uniformly distributed in the halo. Later, we discuss the degree by which the inferred column density underestimates the value if multiple components exist. The most strongly affected line is Mg II λ2803, although the correction to Fe II λ2344 is not negligible.

For a single-component model, we construct a curve of growth assuming the usual Voigt profile with the Doppler parameter taken from the H I line, where b = 56 km s^{-1}. We use the atomic data from Morton (2003) to determine oscillator strengths, statistical weights, and partition functions for each transition (see Spitzer 1978 for details of the curve of growth method). Statistical uncertainties in the equivalent width determination and uncertainty in the Doppler velocity parameter are propagated through to provide column density errors. Additional uncertainties such as those associated with various assumptions are discussed below (e.g., we assume a single line characterized by a single value of b, but there may be multiple lines). The Fe II λ2344 line is close to the linear part of the curve of growth, with a correction factor to the equivalent width of 1.69. The resulting column for Fe II is $\log[N(\mathrm{Fe\,II})/\mathrm{cm}^{-2}] = 14.41 \pm 0.14$, while the upper limit for the Mg I column is $\log[N(\mathrm{Mg\,I})/\mathrm{cm}^{-2}] = 12.67$ (statistical errors only). The Mg II λ2803 line has an optical depth of about 70 at the line center and lies on the flat part of the curve of growth. We calculate a column density of $\log[N(\mathrm{Mg\,II})/\mathrm{cm}^{-2}] = 15.48(+0.36, -0.27)$.

3. RESULTS AND DISCUSSION

To convert the equivalent width to a column density of an element requires a model for both the opacity effects (discussed above) and for the ionization fraction for the particular ionization state. We assume that photoionization controls the ion fractions and that the photons come from the disk of the galaxy. This is certainly not the entire story, as Rand (1998) and Rand

et al. (2008) have shown that photoionization models have difficulty reproducing the optical and infrared emission line data from the halo of NGC 891. They conclude that there is likely to be a secondary source of ionization. Reynolds et al. (1999) reach a similar conclusion for Milky Way halo emission line gas and they suggest that the additional heating could be due to the dissipation of interstellar plasma turbulence.

Even by ignoring this additional heating mechanism, the precise value of the ionization radiation field is only known roughly, with uncertainties from both models and the observational interpretation of emission lines. An important input to the models is the leakage of ionizing radiation from the disk, along with the propagation of UV radiation between the ionization edges of hydrogen (13.6 eV) and the ions Mg I (7.65 eV) and Fe I (7.9 eV), which provides the dominant amount of photoionization for Mg II and Fe II if too little of the radiation above 13.6 eV escapes. The propagation and escape of ionizing radiation has been calculated with various models (e.g., Dove & Shull 1994; Wood et al. 2010) where the result depends on the structure of the ISM and the degree to which radiation propagates through low-density channels where absorption is minimized. These models are constrained by observations, such as by galaxywide emission line observations (e.g., Oey et al. 2007) and by emission line observations directly from the halos of edge-on galaxies (Rand 1998) or from Galactic high-velocity clouds that are irradiated (Putman et al. 2003).

We adopt a simple model for the ionizing and UV radiation reaching 5 kpc in which the shape of the radiation field is given by O stars and the value of the ionization parameter is constrained by Rand (1998). Calculations were performed with Cloudy version C08, most recently described by Ferland et al. (1998). The ionizing photons pass through the halo H I observed by Oosterloo et al. (2007) prior to ionizing the gas at 5 kpc above the disk. We assume that the H I is smoothly distributed at any particular height so that the plane-parallel approximation holds. The radiation softens as it rises upward through the H I layer so that by the time it reaches 5 kpc, most of the radiation above 13.6 eV has been absorbed. From the work of Rand (1998), the ionization parameter U is likely in the range $-6 < \log(U) < -3.5$, from which we calculate that the ionization fractions of Mg II and Fe II exceed >90%. There is a simple explanation for this result in that the H I absorbs most of the photons above 13.6 eV, while the ionization potential for the transition to twice ionized species is 15.0 eV for Mg II and 16.2 eV for Fe II. Therefore, there are ample photons to ionize these elements to their first ionization state but not the second. For this reason, this result is nearly independent of the flux density of radiation emitted from the disk, the vertical form for the structure of the H I, or even the total column of H I, provided they are not orders of magnitude different than observed. There may be complications, discussed below, so for our limiting case, we adopt ionization fractions of 1.0 for these ions.

Emission from ionized gas is detected to heights approaching 5 kpc (Rand et al. 2008), indicating that the Mg and Fe are not entirely singly ionized. Models now try to take into account the complicated non-uniform gaseous structures that would be produced by supernovae (Wood et al. 2010). In their models with high ionizing fluxes, gas is nearly fully ionized at all heights above the plane, in conflict the H I observations showing large amounts of H I above the disk. For models with lower ionizing fluxes, the gas is ionized within 1 kpc of the plane, becoming entirely neutral at greater heights, consistent with our limiting case model.

Another relevant study is the absorption line study toward the globular clusters M3 and M5 at heights of 10 kpc and 5.3 kpc above the plane (Howk & Consiglio 2012). Howk & Consiglio find that nearly all of the S along the sight lines is in the form of S II or S III with 50%–75% of S occurring as S II. The ionization potentials of S I is 10.4 eV, below that of H I but about 3 eV above that of Mg I or Fe I. The ionization potential for S II is 23.3 eV, 7–8 eV above that of Mg II or Fe II so we might estimate that about half of Mg or Fe is not in the form of Mg II or Fe II along these sight lines. We note that this determination of the relative ionization states of S probes a variety of heights from the disk up to the globular clusters, which may not be representative of the ionization state distribution for a sight line at a constant 5 kpc height above the plane. In the following, we determine metallicities for the limiting case (100% of the Mg and Fe are singly ionized), acknowledging that lower ionization fractions would lead to larger metallicities, for Mg and Fe.

Some information is available for the ionized gas column densities at this height in the halo from optical Balmer line emission and from X-ray studies. The X-ray observations show a hot halo of temperature about 3×10^6 K, which is close to the value expected for hydrostatic equilibrium, so it is probably volume-filling (Bregman & Houck 1997). The X-ray emission leads to a density distribution, and along the absorption line of sight closest to the bulge, the column density is 8×10^{19} cm^{-2}, less than the H I column. This gas will not produce UV absorption lines, but it will provide an ambient pressure, which is $p/k \sim 10^4$ K cm^{-3}. This implies that 10^4 K, Balmer-emitting gas would have a density of $\sim$1 cm^{-3}, assuming it is in pressure equilibrium with the X-ray gas. To reproduce the observed Balmer emission line intensity (Rand 1997), the 10^4 K gas only occupies 1% of the volume and has a column density 30 times less than the H I column, so its contribution to the mass can be neglected. Similarly, the H I, probably at $\sim 10^2$ K, would also occupy a small volume but its mass is measured directly and is the dominant component at this height.

We can express the abundances of Mg and Fe relative to their solar abundances, for which we adopt a solar Fe abundance of 7.50 and a solar Mg abundance of 7.60 (Asplund et al. 2009). This leads to [Fe/H] $= -1.18 \pm 0.14$ and [Mg/H] $= -0.23+0.36/-0.27$. These abundances do not take into account the depletion of metals onto grains. Fortunately, Fe and Mg are found to be depleted by different amounts along Milky Way sight lines, with the relative depletion difference being correlated with the total depletion (Savage & Sembach 1996). In all cases, the Fe depletion is greater than that of Mg, with the difference usually a factor of 2–10 (0.3–1.0 in the log). For absorption lines in Milky Way disk + halo gas, the average logarithmic depletion correction for Fe is 0.92 and for Mg is 0.6. Making these corrections, [Fe/H] $= -0.26 \pm 0.14$ and [Mg/H] $= +0.37$ $+0.36/-0.27$. If we were to use the depletion correction factors for warm disk gas, 1.22 for Fe and 0.81 for Mg (in the log), the corrected abundances would be [Fe/H] $= 0.02 \pm 0.14$ and [Mg/H] $= 0.58 +0.36/-0.27$. In either case, the metallicity of the gas is at least half solar and possibly above the solar value.

In this analysis, we assumed that the absorbing material is distributed continuously in the halo so that the line width is determined by the rotational velocity distribution of the halo. If the absorbing gas is confined to a few clouds or sheets, with line widths that are narrow compared to the rotational velocity, and where the lines are not overlapping, the inferred columns for Fe and Mg would be raised. The limiting case would be if the intrinsic thermal lines widths were so narrow that the lines

lie on the damping part of the curve of growth, which can raise the columns by two orders of magnitude. This would lead to a metallicity about two orders of magnitude in excess of the solar value, an unlikely result. Also, this correction would affect Mg more than Fe, so even more modest corrections could lead to highly supersolar values of [Mg/Fe]. For these reasons, we expect that our adopted model is not far from the truth, although the columns could be 2–3 times higher without having to adopt exotic models for the absorbing medium (e.g., an unmixed part of supernova ejecta).

Gas being accreted onto NGC 891 is unlikely to have near-solar abundances. For example, the H I high-velocity gas around the Milky Way known as Complex C, thought to be accretion material, has a metallicity of 0.1–0.3 $Z_{\rm Solar}$ (Tripp et al. 2003). Consequently, we conclude that the gas is from the disk of the galaxy and it has been brought up to a height of 5 kpc by galactic disk processes. This favors a galactic fountain for the origin of the metal-bearing gas. If the disk metallicity in NGC 891 is similar to the Milky Way, this sight line above the inner disk should have a metallicity above the solar value.

There is a considerable literature on Mg II absorption lines seen against background AGN spectra, although they tend to be at much larger impact parameters (e.g., Chen et al. 2010; Kacprzak & Churchill 2011; Bouché et al. 2012). These studies also have significantly higher spectral resolution, which permits them to study the velocity properties of the lines relative to the galaxy. From these studies, the Mg II absorbing material has a higher column density close to the galaxy and our value is consistent with some of the other absorption systems close to galaxies (Chen et al. 2010). This absorbing gas is not simply in rotation around the galaxy and various scenarios are suggested, such as where some of the gas is being accreted along the major axis with outflow along the minor axis (Kacprzak et al. 2012). Present observational limitations prevent us from making such velocity comparisons and due to the edge-on orientation, it will never be possible to comment on inflow versus outflow. However, higher spectral resolution observations will allow one to examine whether this gas is rotating like the H I or involved in some different type of behavior, such as the inflow along a stream of accretion material.

There are a number of improvements that are possible with additional UV absorption line observations. At the resolution of these observations, the lines in NGC 891 are not only unresolved, they are partly blended with weaker Milky Way lines. With higher spectral resolution, we could obtain equivalent widths for five separate Fe II lines, covering a range of f values. With such a set of lines, a more accurate column density is easily obtained, especially in the event that there are multiple components in a line, due to a non-uniform cool gas distribution. With a resolution of 20 km s^{-1} or less, we would be able to resolve the rotation of the galaxy and determine abundances as a function of radial position in the galaxy. Another important improvement would be to accurately determine the depletion factor in the gas. In this paper, we inferred the absolute depletion levels by using the relative depletions of two elements that are primarily not in the gas phase. A better way of measuring the depletion is to use at least one element that is primarily in the gas phase. Low depletions are found in the refractory elements, such as O or S, which have UV resonance lines at wavelengths shorter than the STIS observation presented here. Both of these observational improvements are possible using the COS spectrograph on *HST*.

The authors wish to thank Tom Oosterloo for providing the original H I data. We gratefully acknowledge partial support for this work from NASA, and in particular, through an *HST* grant as well as LTSA and ADAP grants.

REFERENCES

Asplund, M., Grevesse, N., Sauval, A. J., & Scott, P. 2009, ARA&A, 47, 481
Bouché, N., Hohensee, W., Vargas, R., et al. 2012, MNRAS, 426, 801
Bregman, J. N., & Houck, J. C. 1997, ApJ, 485, 159
Bregman, J. N., & Pildis, R. A. 1994, ApJ, 420, 570
Chen, H.-W., Helsby, J. E., Gauthier, J.-R., et al. 2010, ApJ, 714, 1521
Dove, J. B., & Shull, J. M. 1994, ApJ, 430, 222
Eckart, M. E., Stern, D., Helfand, D. J., et al. 2006, ApJS, 165, 19
Ferland, G. J., Korista, K. T., Verner, D. A., et al. 1998, PASP, 110, 761
Harrison, F. A., Eckart, M. E., Mao, P. H., Helfand, D. J., & Stern, D. 2003, ApJ, 596, 944
Heald, G. H., Rand, R. J., Benjamin, R. A., & Bershady, M. A. 2006, ApJ, 647, 1018
Howk, J. C., & Consiglio, S. M. 2012, ApJ, 759, 97
Kacprzak, G. G., & Churchill, C. W. 2011, ApJL, 743, L34
Kacprzak, G. G., Churchill, C. W., & Nielsen, N. M. 2012, ApJL, 760, L7
Knezek, P. M., & Bregman, J. N. 1998, AJ, 115, 1737
Li, J.-T., & Wang, Q. D. 2013, MNRAS, 428, 2085
Miller, E. D., Bregman, J. N., & Knezek, P. M. 2002, ApJ, 569, 134
Miller, E. D., Bregman, J. N., & Seitzer, P. 2000, BAAS, 32, 1454
Miller, E. D., Bregman, J. N., & Wakker, B. P. 2009, ApJ, 692, 470
Morton, D. C. 2003, ApJS, 149, 205
Oey, M. S., Meurer, G. R., Yelda, S., et al. 2007, ApJ, 661, 801
Oosterloo, T., Fraternali, F., & Sancisi, R. 2007, AJ, 134, 1019
Peek, J. E. G., Putman, M. E., & Sommer-Larsen, J. 2008, ApJ, 674, 227
Putman, M. E., Bland-Hawthorn, J., Veilleux, S., et al. 2003, ApJ, 597, 948
Rand, R. J. 1997, ApJ, 474, 129
Rand, R. J. 1998, ApJ, 501, 137
Rand, R. J., Kulkarni, S. R., & Hester, J. J. 1990, ApJL, 352, L1
Rand, R. J., Wood, K., & Benjamin, R. A. 2008, ApJ, 680, 263
Reynolds, R. J., Haffner, L. M., & Tufte, S. L. 1999, ApJL, 525, L21
Sargent, W. L. W., Boksenberg, A., & Steidel, C. C. 1988, ApJS, 68, 539
Savage, B. D., & Sembach, K. R. 1996, ARA&A, 34, 279
Schneider, D. P., Hartig, G. F., Jannuzi, B. T., et al. 1993, ApJS, 87, 45
Silk, J., & Mamon, G. A. 2012, RAA, 12, 917
Spitzer, L. 1978, Physical Processes in the Interstellar Medium (New York: Wiley-Interscience)
Strickland, D. K., Heckman, T. M., Colbert, E. J. M., Hoopes, C. G., & Weaver, K. A. 2004, ApJS, 151, 193
Swaters, R. A., Sancisi, R., & van der Hulst, J. M. 1997, ApJ, 491, 140
Tripp, T. M., Wakker, B. P., Jenkins, E. B., et al. 2003, AJ, 125, 3122
Tüllmann, R., Pietsch, W., Rossa, J., Breitschwerdt, D., & Dettmar, R. 2006, A&A, 448, 43
Vanden Berk, D. E., Richards, G. T., Bauer, A., et al. 2001, AJ, 122, 549
Wakker, B. P. 2004, Ap&SS, 289, 381
Wakker, B. P., & van Woerden, H. 1997, ARA&A, 35, 217
Westmeier, T., Braun, R., & Thilker, D. 2005, A&A, 436, 101
Wood, K., Hill, A. S., Joung, M. R., et al. 2010, ApJ, 721, 1397